Computer Methods and Programs in Biomedicine 224 (2022) 107008

Contents lists available at ScienceDirect

Computer Methods and Programs in Biomedicine

journal homepage: www.elsevier.com/locate/cmpb

Modeling of the cerebral blood circulation in a capillary network accounting for the influence of the endothelial surface layer

Andrey Kovtanyuk[a,*], Varvara Turova[a], Irina Sidorenko[b], Alexander Chebotarev[c], Renée Lampe[a]

[a] Klinikum rechts der Isar, Technische Universität München, Ismaningerstr. 22, München, 81675, Germany
[b] Fakultät für Mathematik, Technische Universität München, Boltzmannstr. 3, Garching bei München, 85747, Germany
[c] Far Eastern Federal University, Far Eastern Center for Research and Education in Mathematics, Ajax Bay 10, Russky Island, Vladivostok, 690922, Russia

ARTICLE INFO

Article history:
Received 3 January 2022
Revised 22 June 2022
Accepted 5 July 2022

Keywords:
Mathematical modeling of cerebral blood circulation
Endothelial surface layer
Finite element method

ABSTRACT

Background and objective: The paper describes a mathematical model of blood flow in capillaries with accounting for the endothelial surface layer (ESL).

Method: The influence of ESL is modeled by a boundary layer with zero flow velocity. Finite element modeling and an analytical approach based on the homogenization of the core region of blood flow occupied by erythrocytes are developed to describe the resistance of a capillary. The reliability of the results obtained is verified for different values of the discharge hematocrit and vessel diameter using known *in vivo* data.

Results: The proposed approach is applied to the numerical simulation of blood circulation in a capillary network of the germinal matrix of infants born at 25 gestational weeks. The influence of the hematocrit level and effective thickness of ESL on the resistance of the capillary network of the germinal matrix of preterm infants is studied. It was found that a decrease in the effective thickness of ESL in the capillary network (and/or a decrease in the hematocrit) leads to reducing the resistance of the capillary network.

Conclusion: A decrease in the effective thickness of ESL in the capillary network leads to an increase in the pressure drop in arterioles, which may be considered as an additional risk factor for hemorrhages in fragile blood vessels within the germinal matrix.

1. Introduction

Realistic modeling of blood circulation in the entire brain requires an adequate mathematical description of blood flow in a single vessel. Assuming the blood to be homogeneous and incompressible, one can model it using the following Poiseuille's law [35]:

$$Q = \frac{\Delta p}{R} := \frac{\pi}{8}\frac{r^4}{L\mu}\Delta p. \tag{1}$$

Here, Q is the blood flow rate, Δp the pressure difference (pressure drop), R the vessel resistance, r the radius of the vessel, L the length of the vessel, μ the dynamic viscosity. Poiseuille's law provides an adequate description of the blood flow in vessels with large enough diameter. For microvessels, e.g. for capillaries, the blood cannot be considered as a homogeneous fluid with a constant viscosity. Instead, it is modeled as plasma with suspended red blood cells (RBCs), also called erythrocytes. Other elements of blood (white blood cells, platelets, etc.) have small volume fractions and give negligible effects on the blood flow. Thus, the blood in a microvessel can be described by a two-phase fluid consisting of plasma and RBCs, wherein the RBCs phase has much higher viscosity compared to plasma phase [4,5]. Numerical modeling of the two-phase blood flow in a capillary can be performed by finite element method applied to Stokes equations [5,19].

The blood flow is characterized by the presence of a layer free of RBCs near the vessel wall. Since the longitudinal velocity decreases towards the vessel wall, the velocities of RBCs are higher than the average blood velocity. This means that there is a difference between the tube hematocrit (the volume fraction of RBCs in the vessel at a given time instant) and the discharge hematocrit (the volume fraction of RBCs collected at the end of the tube at a given time period). The discharge hematocrit is higher than the

* Corresponding author.
E-mail addresses: kovtanyu@ma.tum.de (A. Kovtanyuk), turova@ma.tum.de (V. Turova), sidorenk@ma.tum.de (I. Sidorenko), cheb@iam.dvo.ru (A. Chebotarev), renee.lampe@tum.de (R. Lampe).

https://doi.org/10.1016/j.cmpb.2022.107008
0169-2607/

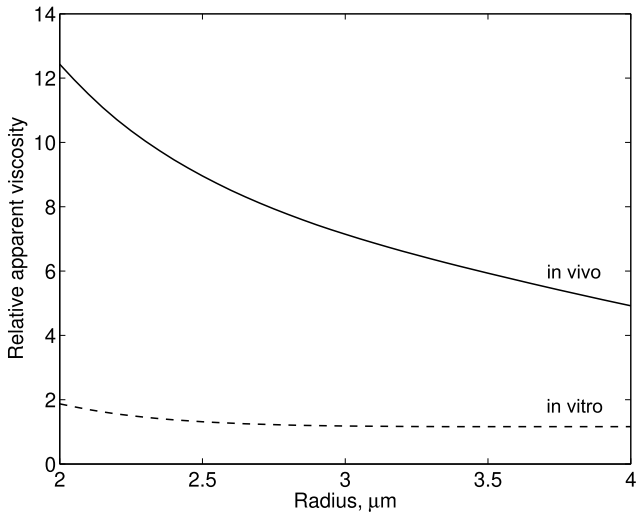

Fig. 1. Dependence of the *in vitro* (dashed line) and *in vivo* (solid line) relative apparent viscosity on the radius of capillary for the discharge hematocrit of 0.3 (obtained by formulas from [28,32]). It is an illustration of the ESL impact on hemodynamics.

tube hematocrit. This phenomenon is called Fåhræus effect [30]. The level of the discharge hematocrit has a significant influence on the characteristics of blood flow in microvessels [31,32,35].

Note that Poiseuille's law does not apply to microvessels. However, to evaluate the resistance to blood flow in capillaries, it is possible, on the base of (1), to define the so-called apparent or effective viscosity of blood, that is, the viscosity of a homogeneous fluid that would give the same blood flow rate for a given capillary radius and pressure drop. According to (1), the apparent viscosity is determined as

$$\mu_{\text{app}} = \frac{\pi}{8}\,\frac{r_c^4}{L}\,\frac{\Delta p}{Q}\,, \tag{2}$$

where r_c is the radius of a capillary.

Experimental measurements of the apparent viscosity are performed *in vitro* and *in vivo*. Usually, *in vitro* data corresponds to blood flow in glass tubes, whereas *in vivo* data is gained from microvessels of animals. In the case of blood vessels with relatively large diameter, the observed behaviour of the apparent viscosity of living vessels is similar to that in glass tubes. However, the values of the apparent viscosity obtained by Lipowsky et al. [20,21] for blood flow in microvessels were much higher than expected from the *in vivo* data.

The dependence of the apparent viscosity on the discharge hematocrit and vessel diameter both *in vitro* and *in vivo* can be found in [28,32], where the corresponding analytical approximations are given. The graphs of the relative apparent viscosity (the ratio of the apparent viscosity to plasma viscosity) corresponding to *in vitro* and *in vivo* data for the discharge hematocrit of 0.3 are shown in Fig. 1.

The observed significant difference between the *in vivo* and *in vitro* data can be explained by the presence of the endothelial surface layer attached to the inner surface of blood vessels, which has a substantial inhibitory effect on the blood flow.

The term "Endothelial surface layer" (ESL) means the layer between vascular endothelium and blood. The ESL thickness is estimated as $\geq 0.5\,\mu$m (approximately equals to $0.5\,\mu$m [10,23,34,43,46] or from 0.5 to 1 μm [30,42]). The ESL includes the glycocalyx, a thin (about 50 nm) layer of membranebound macromolecules. The rest part consisting of absorbed plasma components is often modeled as a porous layer restricting the penetration of large molecules [16,17,39,43,44]. At the same time, usually, a layer of plasma is also considered between the ESL and core region of blood flow occupied by RBCs [23,30,42].

The ESL is characterized by a significantly retarded plasma motion. A. Copley studied the endothelium-plasma interface and developed a concept which assumes the presence of an immobile layer of plasma at the vessel wall [8,9]. A similar approach to describe the influence of ESL on blood flow is considered in [30,31,38].

In the current paper, following the works [8,9,29,31,38], where a significant slowdown or complete absence of flow in ESL is noted, the influence of ESL on the apparent viscosity is investigated by means of the boundary layer with zero velocity (immobile plasma layer). By calculating the blood flow Q for a given pressure drop Δp, we can find the apparent viscosity by formula (2) and compare it with *in vivo* data from [32] to estimate the adequacy of the mathematical model.

Two approaches to find the apparent viscosity are proposed. In the first one, we apply the finite element method to calculate the blood flow and discharge hematocrit (see Section 2.1). In the second one, a homogenization of the core region of blood flow occupied by RBCs is conducted to obtain explicit formulas for hemodynamic characteristics (see Section 2.2). In the both cases, fitting the results of mathematical modeling to experimental data is done by choosing an appropriate thickness of the immobile plasma layer. Note that a preliminary analysis of the influence of ESL on blood flow has been conducted in [19] based on finite element modeling. In the current work, the finite element analysis is performed under the assumption of a different representation of the thickness of RBC free boundary layer which is more correct with respect to experimental data. The comparison of the results obtained in Sections 2.1 and 2.2 demonstrates the adequacy of the analytical approach which can then be used to determine vessels resistances and calculate the cerebral pressure distribution in large capillary networks. In Section 2.3, to simulate the cerebral blood circulation, a vascular system containing 9 levels of arterioles, 9 levels of venules, and a capillary level is considered. Each level of arterioles and venules has a parallel topology, while capillaries are connected by a net-like topology. Using this blood vessel network, the pressure drop at each vascular level can be found. The cerebral vascular system is scaled to the preterm infant brain at 25 gestational weeks, for which further simulations are carried out to study the effect of ESL on pressure drops. In Section 3 ("Results"), the influence of the hematocrit level and effective thickness of ESL on the pressure drop in the capillary network of the germinal matrix of preterm infants at 25 gestational weeks is demonstrated. It is noted that a decrease in the effective thickness of ESL in the capillary network leads to an increase in the pressure drop in arterioles, which may be considered as an additional risk factor for hemorrhages in fragile blood vessels within the germinal matrix.

2. Methods

2.1. Finite element modeling

As it was proposed in [4,5], the RBCs and blood plasma are considered as one flow with two different viscosities, the viscosity of plasma and much larger viscosity of RBCs. Such an approach is motivated by the results of [40] claiming that a rigid body moving in a fluid can be replaced with another fluid whose viscosity tends to infinity. In the following numerical simulations, the viscosity of blood plasma is assumed to be $\mu_1 = 0.001\,\text{Pa}\cdot\text{s}$, whereas the viscosity of RBCs is set to be $\mu_2 = 0.1\,\text{Pa}\cdot\text{s}$ to make RBCs effectively rigid.

The capillary with two-phase blood flow has axial symmetry (see Fig. 2, where the central longitudinal cross section of a capillary is presented). Here, r_c is the radius of the capillary, r_e the

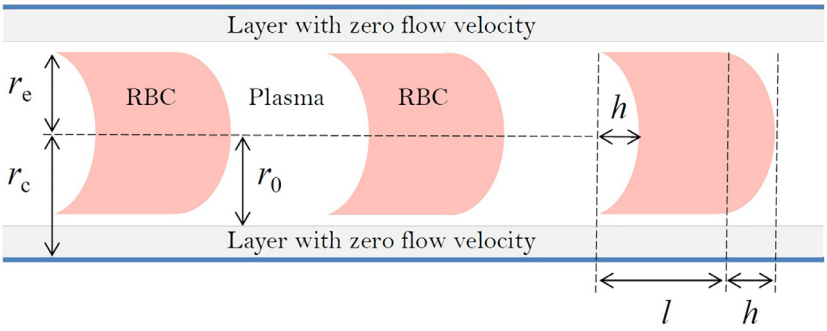

Fig. 2. Schematic drawing of the RBCs moving in a capillary.

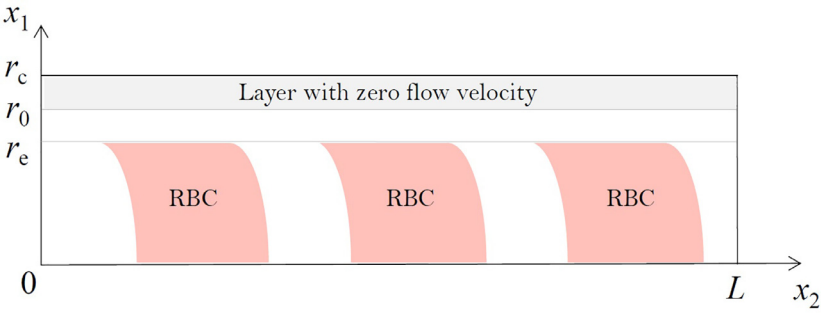

Fig. 3. The computational domain in cylindrical coordinates.

radius of RBCs, l the thickness of RBCs, and the parameter h describes the deformation of RBCs. The arc of the deflection is a parabola which is uniquely determined by the RBC radius and the parameter h. In the undeformed state, the RBC is modeled as a cylinder with a circular cross section.

To take into account the influence of ESL, the presence of a boundary layer with zero flow velocity is assumed (see Fig. 2). Following [31,38], we will call the thickness of the layer with zero flow velocity, $r_c - r_0$, as the effective thickness of ESL. Further, we assume that the flow is steady-state and without transition effects. Therefore, the blood flow in a capillary can be described by the steady-state Stokes equations with space variable viscosity.

Assuming that the flow is axisymmetric, all variables depend on the radial x_1 and longitudinal x_2 coordinates only. Let u_1 and u_2 be the radial and longitudinal flow velocities, respectively, and p the pressure. Therefore, it is possible to reduce the consideration to two dimensional domain $\Omega = (0, r_0) \times (0, L)$ (see Fig. 3).

The corresponding Stokes equations for the velocity $u = (u_1, u_2)$ and pressure p in the domain Ω have the form [41]:

$$-2\nabla \cdot (\mu \mathbf{D}(u)) + \nabla p = 0, \tag{3}$$

$$\nabla \cdot u = 0. \tag{4}$$

Here, $\mathbf{D}$ is the velocity deformation tensor. In cylindrical coordinates, taking into account the axial symmetry, it is defined as

$$\mathbf{D}(u) = \frac{1}{2}\begin{pmatrix} 2\partial u_1/\partial x_1 & 0 & \partial u_1/\partial x_2 + \partial u_2/\partial x_1 \\ 0 & 2u_1/x_1 & 0 \\ \partial u_1/\partial x_2 + \partial u_2/\partial x_1 & 0 & 2\partial u_2/\partial x_2 \end{pmatrix}$$

and

$$\nabla \cdot u = \frac{u_1}{x_1} + \frac{\partial u_1}{\partial x_1} + \frac{\partial u_2}{\partial x_2}.$$

To formulate the boundary conditions, we determine the following parts of the boundary $\partial\Omega$ of the domain Ω:

$$\Gamma_0 = \{x \in \partial\Omega : x_1 = r_0\}, \quad \Gamma_1 = \{x \in \partial\Omega : x_2 = 0\},$$

$$\Gamma_2 = \{x \in \partial\Omega : x_2 = L\}.$$

Further, the system (3) and (4) is supplemented by the following boundary conditions:

$$u|_{\Gamma_0} = 0, \tag{5}$$

$$u_1|_{\Gamma_1} = u_1|_{\Gamma_2} = 0, \tag{6}$$

$$p|_{\Gamma_1} = p_0, \quad p|_{\Gamma_2} = 0. \tag{7}$$

Due to equalities (4) and (6), the following conditions on the component u_2 at the boundaries Γ_1 and Γ_2 hold:

$$\frac{\partial u_2}{\partial x_2}|_{\Gamma_1} = \frac{\partial u_2}{\partial x_2}|_{\Gamma_2} = 0. \tag{8}$$

Let us introduce the spaces V_1, V_2, and Q such that

$$V_1 = \{v \in \mathcal{D}' : x_1^{-1/2} v \in L^2(\Omega),\ x_1^{1/2} \partial v/\partial x_i \in L^2(\Omega),\ i = 1, 2\},$$

$$V_2 = \{v \in \mathcal{D}' : x_1^{1/2} v \in L^2(\Omega),\ x_1^{1/2} \partial v/\partial x_i \in L^2(\Omega),\ i = 1, 2\},$$

$$Q = \{q \in \mathcal{D}' : x_1^{1/2} q \in L^2(\Omega)\},$$

where $\mathcal{D}'$ is the space of distributions on Ω, and consider the space

$$V = \{v = (v_1, v_2) \in V_1 \times V_2,\ v|_{\Gamma_0} = 0,\ v_1|_{\Gamma_1} = v_1|_{\Gamma_2} = 0\}.$$

To obtain the weak form of Eq. (3), we multiply it by the test function $v \in V$ and integrate the result over Ω. Further, taking into account the equality (8) and condition $v_1|_{\Gamma_1} = v_1|_{\Gamma_2} = 0$, we apply the formula of integration by parts. As a result, for $u \in V$, $p \in Q$, the weak form of Eq. (3) accounting for the conditions (5) – (7) is obtained:

$$\int_\Omega \Big(2x_1\, \mu\, \mathbf{D}(u)\mathbf{D}(v) - x_1\, p\, \nabla \cdot v\Big) dx - \int_{\Gamma_1} p_0\, x_1\, v_2\, dx = 0$$
$$\forall v \in V, \tag{9}$$

where

$$\mathbf{D}(u)\mathbf{D}(v) = \frac{\partial u_1}{\partial x_1}\frac{\partial v_1}{\partial x_1} + \frac{1}{2}\left(\frac{\partial u_1}{\partial x_2} + \frac{\partial u_2}{\partial x_1}\right)\left(\frac{\partial v_1}{\partial x_2} + \frac{\partial v_2}{\partial x_1}\right) + \frac{\partial u_2}{\partial x_2}\frac{\partial v_2}{\partial x_2} + \frac{u_1 v_1}{x_1^2}.$$

The weak form of Eq. (4) for $u \in V$, $p \in Q$ is written as

$$\varepsilon \int_\Omega x_1 p\, q\, dx - \int_\Omega x_1 \nabla \cdot u\, q\, dx = 0 \quad \forall q \in L^2(\Omega), \quad \varepsilon \ll 1. \tag{10}$$

Here, the term with the multiplier ε is added to provide the numerical stability of the solution. Thus, the weak formulation of the problem (3) – (7) in cylindrical coordinates (x_1, x_2) consists of Eqs. (9), (10) and the boundary conditions (5) – (7).

The obtained weak formulation of the problem is the basis to apply the Finite Element method. For its implementation, FreeFEM++ package is used [15]. When performing numerical simulations, P2 finite element space is utilized for the approximation of the functions u and v, whereas P1 finite element space is used for the approximation of the functions p and q. To build a computational mesh, a partition into 50 segments with respect to axis Ox_1 and 1000 segments with respect to axis Ox_2 is used. The viscosity distribution μ is equal to 0.001 Pa · s in the plasma part and 0.1 Pa · s in the RBCs part, the parameter $\varepsilon = 10^{-8}$.

To set the value of the pressure drop at a capillary with the length L, first, the pressure drop in the capillary network (pressure difference between inlets and outlets) is estimated. For that, the cerebral flow rate and total resistance of the capillary network are required. According to [45], the cerebral blood flow rate $Q = 600$ ml/min is a realistic value for an adult brain. Moreover, a cerebrovascular network model from [27] yields the total resistance R_T of the capillary system to be equal to 0.1Pa · s/mm^3, which gives the pressure drop to be equal to 1000 Pa (computed as $Q \cdot R_T$). Following [27], where the parallel topology for capillaries with the length of 600 μm and radius of 2.8 μm is utilized, we consider in further modeling that the pressure drop of 1000 Pa corresponds to the capillary length of 600 μm. Therefore, for the capillary length equals to L, the pressure drop is $5L/3$ Pa. In the numerical modeling, the capillary length is chosen in the range from 50 to 150 μm in accordance with the number of the accounted RBCs.

When conducting computer simulations, along with specifying the radius of the vessel, it is required to determine the radius r_e of the core region of blood flow occupied by RBCs and the linear dimensions of RBCs. Assuming the average thickness of ESL of 0.5 μm [10,23,34,43,46], the ability of ESL to deform [43], and a monotonic dependence of ESL thickness on the capillary radius for $r_c \le 5\,\mu$m [31], the following approximation for r_e (units in μm) can be used:

$$r_e = 0.9 r_c - 0.2. \tag{11}$$

The length l of an erythrocyte is determined by its mean volume equals to 88 μm^3 [25] and the value of r_e, that is $l = 88/\pi r_e^2$ (units in μm). The RBC deformation parameter h (see Fig. 2) is set to $l/3$. Note that small variations of the parameter h do not significantly affect the capillary resistance. The results of finite element modeling presented in the article [5] demonstrate fairly close values of the capillary resistances for $h = l/3$ and $h = 0$.

Following [8,9,29,31,38], where a significant slowdown or even complete absence of flow in ESL is noted, we assume zero flow velocity in the boundary layer $r_0 \le r \le r_c$ $(r_0 > r_e)$ to account for the influence of ESL in microvessels.

To fit the results of finite element modeling to *in vivo* data from [32], the following representation of the boundary of the layer with zero flow velocity (units in μm) is used:

$$r_0 = 0.014453\, r_c^2 + 0.855844\, r_c - 0.157609. \tag{12}$$

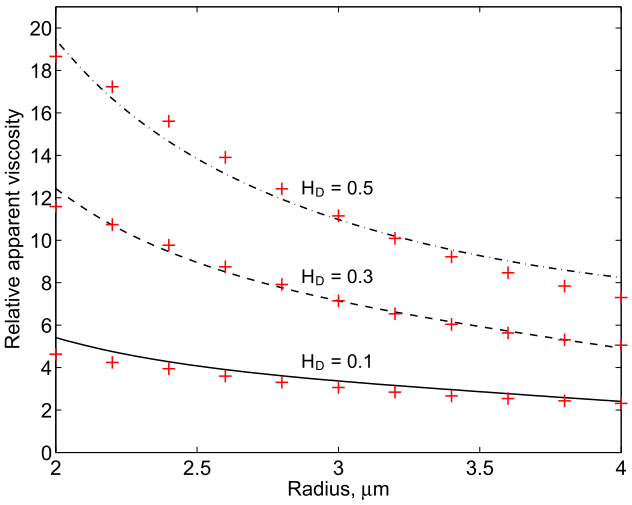

Fig. 4. *In vivo* data of the relative apparent viscosity (obtained by formula from [32]) for different values of the discharge hematocrit: $H_D = 0.1$ (solid plot), $H_D = 0.3$ (dashed plot), and $H_D = 0.5$ (dash-dotted plot); and the corresponding results of the finite element modeling (crosses) using the approximations (11) and (12). (For interpretation of the references to colour in this figure legend, the reader is referred to the web version of this article.)

The formula (12) is obtained by the minimization of the mean square deviation between the apparent viscosities corresponding to *in vivo* data and finite element modeling for the value of discharge hematocrit of 0.3. Note that the representation (12) is obtained under the assumption of the consistency of the approximation (11). Refining the formula (11) will result in a corresponding adjustment of the formula (12). Therefore, from the point of view of mathematical modeling, some change in presentation of r_e is not important since later the numerical results are scaled by the thickness of the layer with zero velocity.

The computed values of the relative viscosity and *in vivo* data calculated by an analytical approximation from [32] are compared in Fig. 4. Note that although the formula (12) was developed using the data for $H_D = 0.3$, it provides a good approximation also for $H_D = 0.1$ and $H_D = 0.5$.

2.2. Analytical approach based on the homogenization of the core region of blood flow occupied by erythrocytes

An alternative approach to find the apparent viscosity is the homogenization of the core region of blood flow $(x_1 < r_e)$ occupied by erythrocytes. This allows us to construct an analytical formula for the apparent viscosity, and further to obtain explicit presentations for the blood flow and resistance of a capillary.

To apply this approach, we neglect the deformation of erythrocytes, that is we consider the medium structure as it is shown in Fig. 5 (instead of the structure demonstrated in Fig. 3). Also, we assume that the pressure depends on the variable x_2 only, that is

$$p = p(x_2). \tag{13}$$

Further, we replace the core region of the blood flow with variable viscosity with a homogenized medium with constant viscosity (see Fig. 6).

The viscosity of the homogenized core region can be found from the condition of equality of the resistances of capillaries demonstrated in Figs. 5 and 6. According to [5], under the assumption (13) and taking into account the presence of the layer with zero flow velocity, the specific resistance R of the capillary shown

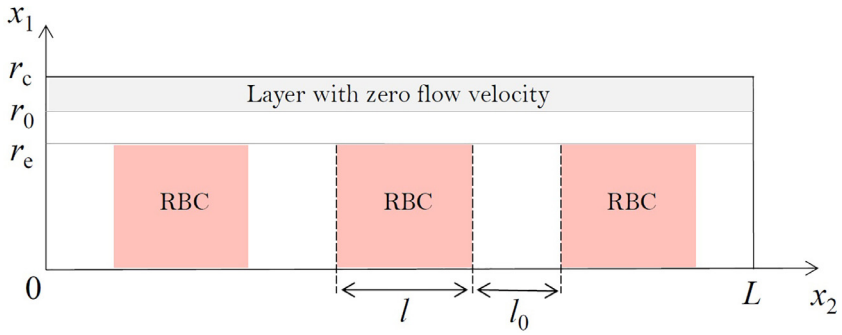

Fig. 5. The computational domain in cylindrical coordinates for the case where the deformation of erythrocytes is neglected.

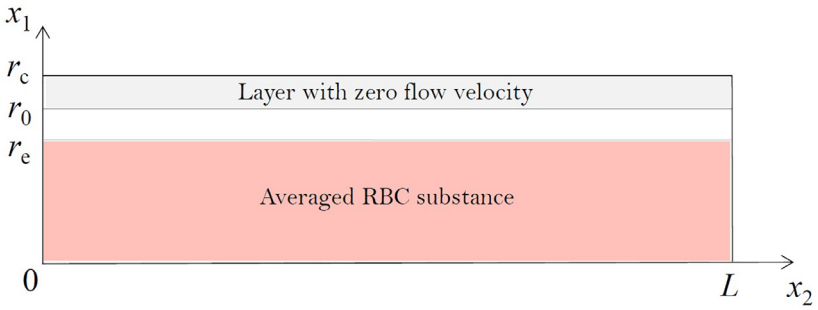

Fig. 6. The computational domain in cylindrical coordinates for the case of a homogenized core region of blood flow occupied by erythrocytes.

in Fig. 5 is determined by the formula

$$R = \frac{8(1-H)}{\pi}\left(\frac{r_0^4}{\mu_1}\right)^{-1} + \frac{8H}{\pi}\left(\frac{r_0^4 - r_e^4}{\mu_1} + \frac{r_e^4}{\mu_2}\right)^{-1}. \tag{14}$$

Here, the parameter $H := l/(l+l_0)$ is the RBC linear density [22], where l is the length of erythrocyte and l_0 the thickness of the plasma gap between adjacent erythrocytes (see Fig. 5). Note that the tube hematocrit is obtained by multiplying H by $(r_e/r_c)^2$.

On the other hand, the specific resistance R^* of the capillary shown in Fig. 6 is determined as

$$R^* = \frac{8}{\pi}\left(\frac{r_0^4 - r_e^4}{\mu_1} + \frac{r_e^4}{\mu_2^*}\right)^{-1}. \tag{15}$$

By equating (14) and (15), the averaged viscosity μ_2^* of the core region of blood flow is

$$\mu_2^* = r_e^4\left(\frac{8}{\pi R} - \frac{r_0^4 - r_e^4}{\mu_1}\right)^{-1}. \tag{16}$$

Using (16) and following [4], the blood flow in the capillary of length L shown in the Fig. 6 at the pressure drop Δp is calculated as

$$Q = \frac{\pi \Delta p}{8L}\left(\frac{r_0^4 - r_e^4}{\mu_1} + \frac{r_e^4}{\mu_2^*}\right). \tag{17}$$

Accordingly, the apparent viscosity is determined as

$$\mu_{\text{app}} = r_0^4\left(\frac{r_0^4 - r_e^4}{\mu_1} + \frac{r_e^4}{\mu_2^*}\right)^{-1}. \tag{18}$$

With that, the analytical presentation for the discharge hematocrit H_D is

$$H_D = H\left(\frac{r_0}{r_c}\right)^2\left(\frac{2(r_0^2 - r_e^2)r_e^2}{\mu_1} + \frac{r_e^4}{\mu_2^*}\right)\left(\frac{r_0^4 - r_e^4}{\mu_1} + \frac{r_e^4}{\mu_2^*}\right)^{-1}. \tag{19}$$

Using (14), (16), (18), and (19), we can calculate the relative apparent viscosity for different values of the discharge hematocrit and radius of capillary. To fit the results to *in vivo* data from [32], we use the following representation of the boundary of the layer with zero flow velocity (units in μm):

$$r_0 = 0.007656\, r_c^2 + 0.885063\, r_c - 0.188294. \tag{20}$$

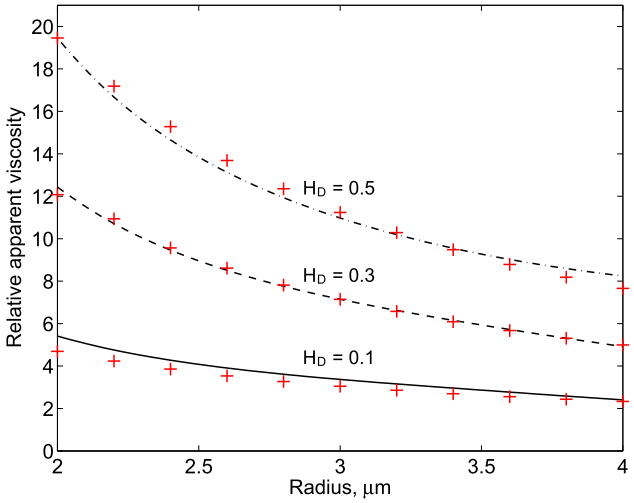

Fig. 7. *In vivo* data of the relative apparent viscosity (obtained by formula from [32]) for different values of the discharge hematocrit: $H_D = 0.1$ (solid plot), $H_D = 0.3$ (dashed plot), and $H_D = 0.5$ (dash-dotted plot); and the corresponding results from the analytical approach (cross) using the approximations (11) and (20).

A comparison of the obtained values of the relative apparent viscosity with *in vivo* data from [32] is presented in Fig. 7.

From the analysis of the results presented in Figs. 4 and 7, it can be concluded that the analytical approach gives a somewhat better approximation of the apparent viscosity compared to the approximation based on the finite element models. In more details, the mean square deviations between the results of the finite element modeling and *in vivo* data for the values of the dis-

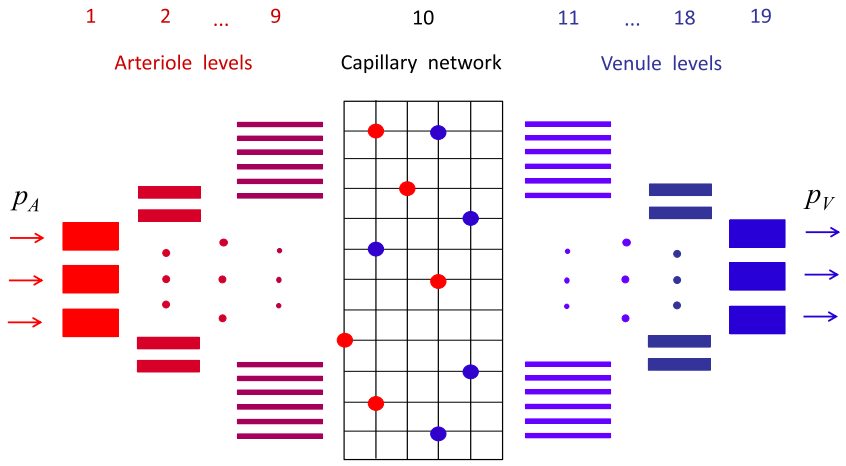

Fig. 8. A modification of Piechnik's vascular brain model. In opposite to [27], the capillary level has a specified net-like topology.

charge hematocrit of 0.1, 0.3, and 0.5 are equal to 0.373, 0.391, and 0.646, respectively. At the same time, the mean square deviations between the results of the analytical approach and *in vivo* data for the values of the discharge hematocrit of 0.1, 0.3, and 0.5 are equal to 0.376, 0.14, and 0.404, respectively.

Note that, due to fitting the thickness of the immobile plasma layer conducted in Sections 2.1 and 2.2, the proposed methods based on the finite element modeling and on the analytical approach provide the calculation of an adequate value of the apparent viscosity, despite of some deviations between the RBCs radius obtained by the formula (11) and experimental data. As a result, this gives a good approximation for the capillary resistances which is necessary to simulate blood circulation in a vascular network.

2.3. Numerical simulation of blood circulation in large capillary networks

In 2008, Piechnik et al. [27] have proposed a model of the brain vascular system consisting of nineteen compartments: nine levels of arterioles, nine levels of venules, and one level of capillaries. Vessels in each level have the parallel topology. The lengths, diameters of the vessels, as well as their number at each level are selected so that the results of numerical simulation of the intravascular pressure and flow velocity are consistent with the experimental data presented in papers [3,12,47]. In [4], a modification of Piechnik's model has been considered. In the modified model of the cerebral vascular system, only the capillary level is changed (see Fig. 8). Although the number of capillaries for the adult brain is the same as in [27], namely 756 millions, the capillary system is generated with a specific netlike n-edge topology for a given $n \in \{3, 4, 5, 6\}$. Additionally, it is supposed that the length and radius of capillaries are random variables distributed around mean statistical values of 63.3 μm and 3.28 μm, respectively (see [7], M2 data). Note that the generated capillary lengths are about 10 times less than the capillary length in Piechnik's model.

To generate the capillary network with n-edge topology, first, the set of all nodes, (i, j, k), $0 \le i < q$, $0 \le j < m$, $0 \le k < l$, is determined. The values q, m, and l are chosen so that the total number of nodes qml corresponds to the required number of edges in the capillary network and the kind of topology used. For an internal node (i, j, k) the adjacent nodes, $(i+1, j, k)$, $(i, j+1, k)$, and $(i, j, k+1)$), are considered, and $[n/2]$ (the integer part of $n/2$) of them are randomly chosen. These nodes are to be connected to (i, j, k) with the corresponding edges (capillaries). If n is odd, then an additional outgoing edge is set with the probability of 0.5. As a result, the average number of edges corresponding to the internal nodes is equal to n. For the boundary nodes, the algorithm may give less than n number of outgoing edges, but the average edge number for a single node through the entire network is close to n.

Similar to paper [4], it is supposed that the network contains blood sources and sinks (inlets and outlets) distributed over the network (see the filled circles at some nodes of the capillary network in Fig. 8). They are associated with the arteriolar and venular endpoints, respectively. The calculation of the total resistance is performed by the direct computation of the total blood flux through the capillary network by analogy with electric circuits, i.e. using Kirchhoff's law and solving a large sparse system of linear algebraic equations [4]. The parameters n and H defining the kind of topology and the RBC linear density, respectively, are selected such that the calculated total resistance of the capillary network is close enough to data obtained by Piechnik's model approximating the results of experimental measurements.

To determine the kind of the topology and the RBC linear density, for different values of parameters n and H, we find the total resistance of the adult brain's capillary network containing 756 millions edges. Then the results are compared with the resistance of the capillary level obtained by applying Piechnik's model, that is with the value of $0.99 \cdot 10^8\,\mathrm{Pa \cdot s/m^3}$. The total resistance of the capillary network for 4-, 5-, and 6-edges topology and different values of the parameter H is shown in Fig. 9. As it is seen from the figure, for certain values of the parameter H, each topology is consistent with the results obtained by Piechnik's model. In more detail, for 4-edge topology, $H = 0.108$; for 5-edge topology, $H = 0.185$; for 6-edge topology, $H = 0.267$. Therefore, in subsequent numerical experiments, we can use any of the above topologies with the corresponding value of the parameter H.

Using the model with a net-like topology allows us to obtain the spatial distribution of pressure in the capillary network of the brain with inhomogeneous structure to predict different abnormal situations. This is especially important in the case of subependymal germinal matrix, which is a specific part of immature brain with high vascularity and fragile vessels. The hemorrhage in vessels of the germinal matrix leads to a disruption of oxygen transport to the brain cells.

To adapt the modified vascular model to preterm infants, for each i-th non-capillary level (i.e. $i \neq 10$) the numbers of vessels, their lengths, and their diameters are reduced by dividing the values from [27] over

$$12 - 1.22\,|i-10|, \quad 1 + 0.14\,|i-10|, \quad 1 + 0.11\,|i-10|, \qquad (21)$$

respectively. This allows us to fit CBF to a typical value corresponding to the infant brain at 25 gestational weeks evaluated as

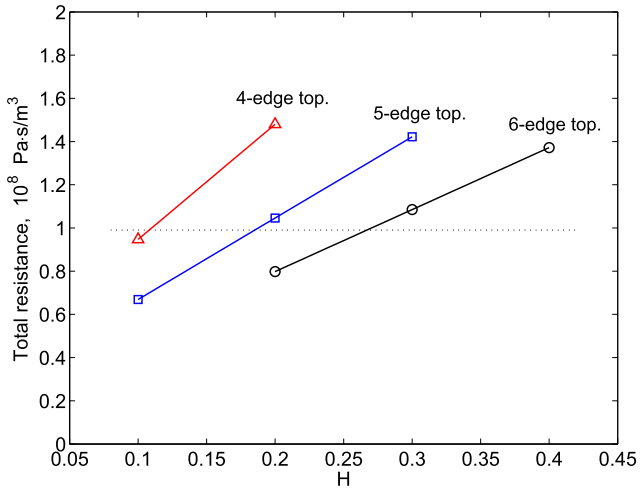

Fig. 9. The total resistance of the brain capillary network for different values of H: line with triangle markers – the case of 4-edge topology; line with square markers – the case of 5-edge topology; line with circle markers – the case of 6-edge topology. Dotted line – Piechnik's model based on experimental data [27].

Table 1
Parameters of the vascular network model for the adult brain [27] / infant brain at 25 gestational weeks.

Vascular level	Number of vessels	Length (mm)	Diameter (mm)
1	10 / 10	86.2 / 38.14	1.92 / 0.965
2	70 / 31	43.1 / 20.33	0.96 / 0.511
3	490 / 142	21.5 / 10.86	0.48 / 0.271
4	3430 / 733	10.8 / 5.87	0.24 / 0.145
5	2.40e+04 / 4.07e+03	5.4 / 3.18	0.12 / 0.077
6	1.92e+05 / 2.70e+04	2.7 / 1.73	0.06 / 0.042
7	1.47e+06 / 1.76e+05	1.4 / 0.99	0.03 / 0.023
8	5.01e+06 / 5.24e+05	0.9 / 0.70	0.02 / 0.016
9	3.84e+07 / 3.56e+06	0.5 / 0.44	0.01 / 0.009
10	7.56e+08 / 6.30e+07	0.6 / 0.6	0.0056 / 0.0056
11	3.84e+07 / 3.56e+06	0.5 / 0.44	0.015 / 0.014
12	5.01e+06 / 5.24e+05	0.9 / 0.70	0.03 / 0.025
13	1.47e+06 / 1.76e+05	1.4 / 0.99	0.045 / 0.034
14	1.92e+05 / 2.70e+04	2.7 / 1.73	0.09 / 0.063
15	2.40e+04 / 4.07e+03	5.4 / 3.18	0.18 / 0.116
16	3430 / 733	10.8 / 5.87	0.36 / 0.217
17	490 / 142	21.5 / 10.86	0.72 / 0.407
18	70 / 31	43.1 / 20.33	1.44 / 0.766
19	10 / 10	86.2 / 38.14	2.88 / 1.447

10 ml/100g/min [24]. The parameters of the vascular systems corresponding to the adult and infant brains are presented in Table 1. As in Piechnik's model, the cerebrovascular system of the preterm infant has the same number of arterioles and venules at the levels that are symmetrical with respect to the capillary level. The suggestion that capillaries of neonates and adults are similar is based on available data for animals [13]. The ratio between the number of vessels of the adult and infant brain at each level is maximal for the capillary compartment and it becomes the smaller, the larger the arterioles and venules are. This reflects a trend towards an increase in microvascular branching in the first postnatal months with further stabilization [14].

In the proposed vascular model of the preterm infant brain, the capillary level is assumed to be consisting of two parallel networks corresponding to the germinal matrix and the rest part of the brain, respectively. Therefore, the total resistance of the capillary network

$$R_{10} = \left(R_{GM}^{-1} + R_B^{-1}\right)^{-1}, \tag{22}$$

where R_{GM} is the resistance of the germinal matrix and R_B the resistance of the rest part of the infant brain. To calculate the resistances R_{GM} and R_B, the direct computation of the total blood flow through the capillary network is performed by using Kirchhoff's law. As a result, the algorithm reduces to solving a large sparse system of linear algebraic equations [4].

When calculating the total blood flow, the number of capillaries in the germinal matrix and rest part of the infant brain is determined as

$$N_{GM} := N_A \kappa \gamma w / w_A, \quad \text{and} \quad N_R := N_A (1-\gamma) w / w_A,$$

respectively. Here, w_A is the weight of the adult brain, w the weight of the infant brain, γ the weight fraction of the germinal matrix, κ the capillary density correction factor for the germinal matrix, $N_A = 756\,000\,000$ the number of capillaries of the adult brain [27]. For infants born at 25 gestational weeks, we set $w = 0.1$ kg [1], $\gamma = 0.023$ [18], $\kappa = 1.5$ [2]. As a result, the number of capillaries in the germinal matrix and rest part of the brain is evaluated as 2.17 and 61.55 million, respectively. The values of the arterial and venous pressure are set as $p_A = 34$ mmHg and $p_V = 5$ mmHg [36,37].

The resistances on the arteriolar and venular levels are calculated as

$$R_i = \frac{8 L_i \mu}{\pi r_i^4 N_i}, \quad i \neq 10, \tag{23}$$

where r_i is the radius of the vessel, L_i the length of the vessel, N_i the number of vessels at the i-th level, and μ the apparent viscosity.

The total resistance of the brain vascular system is determined as

$$R_T = \sum_{i=1}^{19} R_i, \tag{24}$$

and the total flow is calculated by the formula:

$$Q = (p_A - p_V)/R_T, \tag{25}$$

where p_A and p_V are the arterial and venous pressures.

Finally, the pressure drop in the i-th vascular level is found by the equality:

$$\Delta p_i = Q R_i. \tag{26}$$

3. Results

It is worth to note that accounting for the influence of ESL through the layer with zero flow velocity is characterized by a significant increase of the relative viscosity and, respectively, by a proportional increase of the microvessel resistance. As a consequence, it leads to a proportional decrease in the longitudinal velocity under a constant value of the pressure drop in the capillary. The results of the numerical modeling based on the analytical approach are presented in Fig. 10. The velocity profile for the vessel with the diameter 6 μm and $H_D = 0.1$ is shown. In the example considered, accounting for the ESL leads to the 3.6-fold decrease in the blood flow under a constant value of the pressure drop in the capillary. If the value of the blood flow is constant, the effect of ESL leads to the 3.6-fold decrease in the pressure drop.

In the numerical simulations conducted in the framework of the proposed model and parameters used, the effect of a decrease in the hematocrit and effective thickness of ESL on the resistance of the capillary network of infants at 25 gestational weeks was studied. A change in the resistance leads to the proportional change in the pressure drop. In Fig. 11, a linear dependence of the resistance of the capillary network on a decrease of the hematocrit is shown.

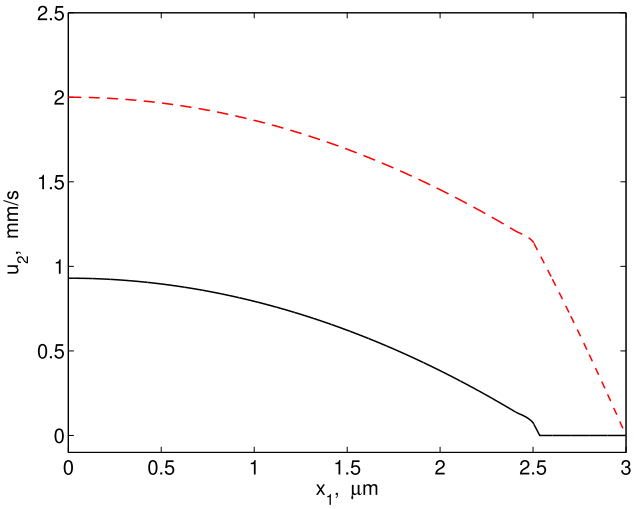

Fig. 10. Velocity profile (longitudinal velocity, u_2) for the vessel diameter of 6 μm and $H_D = 0.1$: with accounting for zero flow velocity layer (solid line) and without it (dashed line).

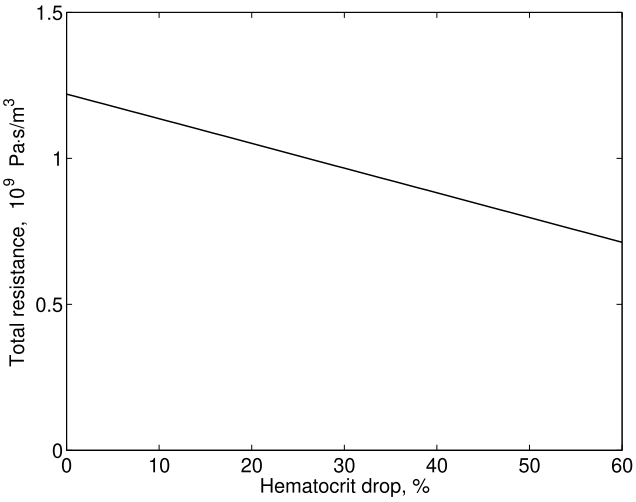

Fig. 11. The total resistance of the capillary network corresponding to the infant at 25 gestational weeks versus the tube hematocrit drop.

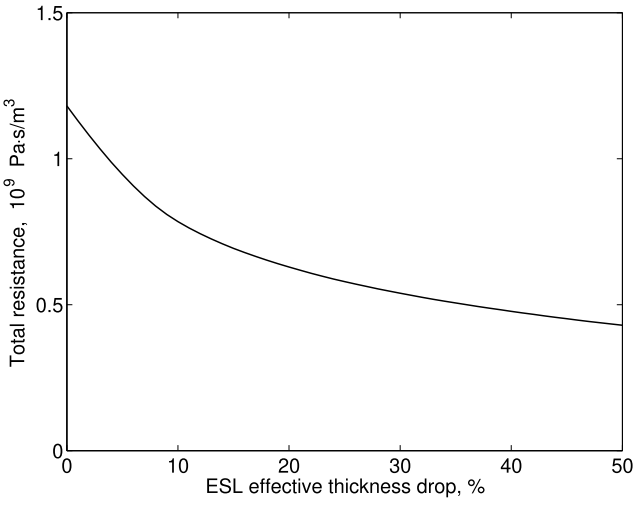

Fig. 12. The total resistance of the capillary network corresponding to the infant at 25 gestational weeks versus the ESL effective thickness drop.

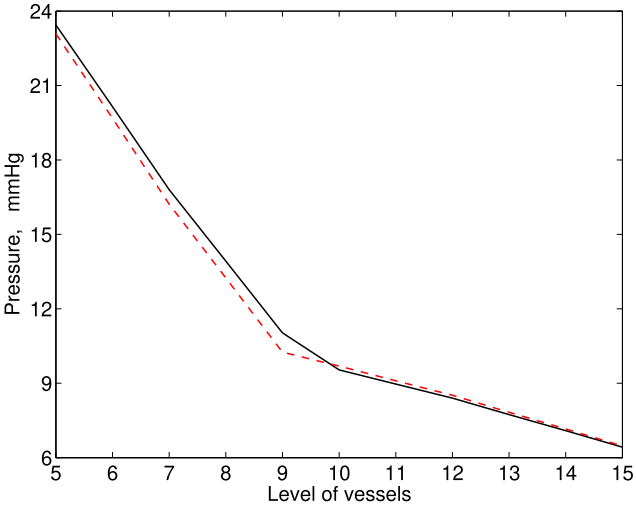

Fig. 13. The cerebral pressure corresponding to the infant born at 25 gestational weeks for different levels of vessels: solid line – the case of normal effective thickness of ESL; dashed line – the case of 2 times reduced effective thickness of ESL.

For example, a 50% decrease in the hematocrit leads to a 29% reduction in the resistance of the capillary network.

Further, the effect of a decrease in the effective thickness of ESL, $r_c - r_0$, was considered. A decrease in the effective thickness of ESL also leads to reducing the resistance of the capillary network (see Fig. 12). So, a 50% decrease in the effective thickness of ESL leads to a 64% reduction in the resistance of the capillary network which results in a 2.7 decrease of the pressure drop at the capillary level.

The decrease in the pressure drop in the capillaries causes an increase in the pressure drop in the arterioles and venules. To demonstrate this, the cerebral pressures for the case of normal and 2 times reduced effective thicknesses of ESL in the capillary network corresponding to the brain of preterm infants at 25 gestational weeks were calculated (see Fig. 13), using the algorithm for finding the resistance of the capillary network [4] and formulas (22) – (26). The decrease in the effective thickness of ESL leads to a slight elevation of the pressure drop in venules and a more noticeable increase in the pressure drop in arterioles (from 23 up to 24 mmHg, that is about 4%) under a constant difference between the arterial and venous pressure, $p_A - p_V = 29$ mmHg (typical for infants born at 25 gestational weeks [36,37]). The elevation of the pressure drop in arterioles may be an additional risk factor for developing brain hemorrhage in preterm infants when being superimposed, for example, with an increased blood pressure, which is transmitted to the fragile blood vessels within the germinal matrix and can result in their rupture [26]. Note that although hemorrhages in preterm infants are more often observed in capillaries and venules, some studies indicate also cases of hemorrhages in arterioles [6,11]. A decrease in the hematocrit level in addition to the reduced effective thickness of ESL will cause a further increase in the pressure drop in arterioles and venules.

4. Discussion

4.1. Effective thickness of ESL

In the approaches based on finite element modeling and homogenization of the core region of blood flow, we use the different approximations for the value of r_0 (see (12) and (20)). The effec-

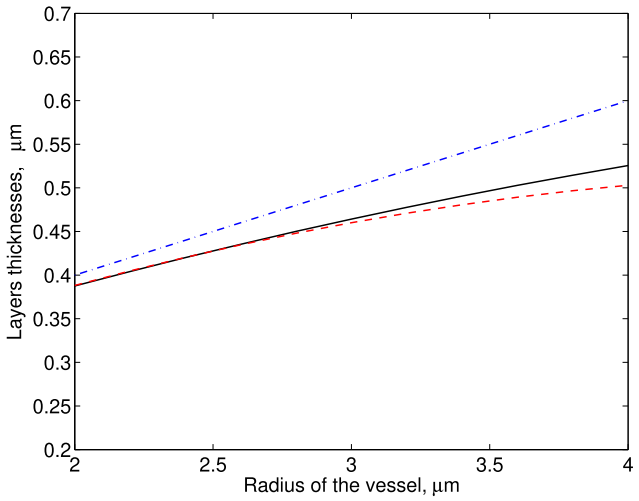

Fig. 14. The effective thickness obtained by the analytical approach (solid line) and by the finite element modeling (dashed line) in compare with the thickness of RBC free layer (dash-dotted line).

tive thicknesses of ESL corresponding to the both approaches and thickness of RBC free layer are shown in Fig. 14.

The deviation in the obtained effective thicknesses is explained by the fact that the condition (13) is more adequate for smaller radiuses. With increasing radius the deviation grows. The deviation compensates simplifying assumptions made to derive the analytical representations (14), (16), and (18).

The simulated effective thicknesses range from 0.39 to 0.53 μm. Similar values (from 0.3 to 0.5 μm) of the effective thickness of ESL were obtained in [38] for venules with the radius of 12 – 21 μm, using mathematical modeling based on the fluorescent microparticle image velocimetry data. In more detail, when the ESL is considered as impermeable (with zero flow velocity), the effective thickness is 0.33 ± 0.04 μm, and in the case of a reduced flow velocity in ESL caused by a high hydraulic resistivity, the effective thickness increases to 0.44 ± 0.04 μm.

Note that, for the capillary radius from 2 to 4 μm, the effective thickness of ESL presented in [31] varies in the intervals (0.28, 0.99), (0.34, 1.17), and (0.39, 1.35) (units in μm) for the discharge hematocrit of 0.1, 0.3, and 0.5, respectively. This is significantly different from the values of the effective thicknesses shown in Fig. 14. The difference is explained by the fact that the blood flow in [31] is homogeneous, while in the present work the blood substance is described as a two-phase medium. Thus, the effective thickness is defined by the chosen mathematical model and provides an adequate description of blood flow in microvessels.

4.2. ESL thickness and hematocrit level of preterm infants

Reduced thicknesses of ESL and decreased hematocrit levels (see Section 3) are often observed in preterm infants. In this regard it is worth mentioning the work [33], where medical data of neonates are given. The neonates are divided into 3 groups: preterm infants born before 30 weeks of gestation (group A), preterm infants born between 30 and 36 weeks of gestation (group B), and term infants (≥ 37 weeks of gestation). An estimate of the change in ESL thickness can be made on the base of the presented data on the size of the perfused boundary region (PBR) which characterizes the penetration of RBCs into ESL. Thus, an increase (decrease) in the size of PBR means a decrease (increase) in the thickness of ESL. From the results of [33] it follows that the ESL thickness in neonates of group A decreases for several weeks after their birth, and when they reach 32 – 34 weeks of gestation, it becomes noticeably less than the ESL thickness in neonates of group B measured at 32 – 36 gestational weeks and in term neonates in the first days after birth (see [33, Figs. 3(a), 4(c)]). The presented data on the PBR values justify the above consideration of up to two times reduced effective thicknesses of ESL in preterm infants.

Also, premature infants are characterized by a low hematocrit. In more detail, the mean value of venous hematocrit in premature infants measured at 30 gestational weeks is 0.48, while in term infants at 40 gestational weeks it is 0.55 (see [33, Table 2]). In preterm neonates of group A in the following days after birth, a decrease in the hematocrit is observed: it is 0.47 and 0.41 at 7 and 26 postnatal day of life, respectively (see [33, Suppl. Table 5]). This corresponds to a 25% decrease in the hematocrit level compared to term infants.

5. Conclusion

A mathematical model of blood flow in a capillary containing the endothelial surface layer has been proposed. The ESL influence is described by the presence of the boundary layer with zero flow velocity. An analytical approach based on the homogenization of the core region of blood flow occupied by erythrocytes to describe the resistance of a capillary has been developed. The reliability of the results obtained has been verified for different values of the discharge hematocrit and vessel diameter using experimental data from the literature. The analytical approach can be used in large vascular networks containing tens or hundreds of millions of capillaries to describe the cerebral blood circulation. A choice of the cerebral vascular model parameters for fitting the resistance value of the capillary network to experimental data has been fulfilled. The numerical simulations of blood circulation in a capillary network of the germinal matrix of infants at 25 gestational weeks have been conducted. The influence of a decrease in the hematocrit and effective thickness of ESL on the resistance of the capillary network of the germinal matrix has been studied. It was noted that a decrease in the effective thickness of ESL in the capillary network leads to an increase in pressure drop in the arterioles, which may be an additional factor increasing the risk of hemorrhage in fragile blood vessels within the germinal matrix of preterm infants.

Funding

This work was supported by the Klaus Tschira Foundation (Grant 00.302.2016), Buhl-Strohmaier Foundation, and Würth Foundation.

Declaration of Competing Interest

The authors have no conflict of interest.

References

[1] J.G. Archie, J.S. Collins, B.R. Lebel, Quantitative standards for fetal and neonatal autopsy, Am. J. Clin. Pathol. 126 (2) (2006) 256–265.
[2] P. Ballabh, A. Braun, M. Nedergaard, Anatomic analysis of blood vessels in germinal matrix, cerebral cortex, and white matter in developing infants, Pediatr. Res. 56 (1) (2004) 117–124.
[3] J.A. Bevan, W. Halpern, M.J. Mulvany, The Resistance Vasculature, Humana Press, Totowa, NJ, 1991.
[4] N.D. Botkin, A.E. Kovtanyuk, V.L. Turova, I.N. Sidorenko, R. Lampe, Direct modeling of blood flow through the vascular network of the germinal matrix, Comp. Biol. Med. 92 (2018) 147–155.
[5] N.D. Botkin, A.E. Kovtanyuk, V.L. Turova, I.N. Sidorenko, R. Lampe, Accounting for tube hematocrit in modeling of blood flow in cerebral capillary networks, Comp. Math. Meth. Med. 2019 (2019) 4235937.
[6] W.D. Brown, G.W. Gerfen, L.A. Vachon, M.D. Nelson Jr., Real-time ultrasonography of arterial IVH in preterm infants, Pediatr. Neurol. 11 (4) (1994) 325–327.
[7] F. Cassot, F. Lauwers, C. Fouard, S. Prohaska, V. Lauwers-Cances, A novel three-dimensional computer-assisted method for a quantitative study of microvascular networks of the human cerebral cortex, Microcirculation 13 (2006) 15–32.

[8] A.L. Copley, Hemorheological aspects of the endothelium-plasma interface, Microvasc. Res. 8 (1974) 192–212.
[9] A.L. Copley, The endoendothelial fibrin lining, fibrinogen gel clotting, and the endothelium-blood interface, Ann.N. Y. Acad. Sci. 416 (1983) 377–396.
[10] E.R. Damiano, The effect of the endothelial-cell glycocalyx on the motion of red blood cellsthrough capillaries, Microvasc. Res. 55 (1998) 77–91.
[11] H.S. Ghazi-Birry, W.R. Brown, D.M. Moody, V.R. Challa, S.M. Block, D.M. Reboussin, Human germinal matrix: venous origin of hemorrhage and vascular characteristics, Am.J. Neuroradiology 18 (2) (1997) 219–229.
[12] R.W. Gore, Pressures in cat mesenteric arterioles and cappilaries during changes in systemic arterial blood pressure, Circ. Res. 34 (1974) 581–591.
[13] S.D. Gray, Morphometric analysis of skeletal muscle capillaries in early spontaneous hypertension, Microvasc. Res. 27 (1) (1984) 39–50.
[14] R. Harb, C. Whiteus, C. Freitas, J. Grutzendler, In vivo imaging of cerebral microvascular plasticity from birth to death, J. Cerebral Blood Flow & Metabolism 33 (1) (2013) 146–156.
[15] F. Hecht, New development in freefem++, J. Numer. Math. 20 (3–4) (2012) 251–265.
[16] C.B. Henry, B.R. Duling, Permeation of the luminal capillary glycocalyx is determined by hyaluronan, Am.J. Physiol 277 (1999) H508–H514.
[17] C.B. Henry, B.R. Duling, TNF-alpha increases entry of macromolecules into luminal endothelial cell glycocalyx, Am. J. Physiol. Heart Circ. Physiol. 279 (2000). H2815–H2823
[18] Y. Kinoshita, T. Okudera, E. Tsuru, A. Yokota, Volumetric analysis of the germinal matrix and lateral ventricles performed using MR images of postmortem fetuses, 2001, AJNR Am. J. Neuroradiol, 22, 2, 382–388
[19] A. Kovtanyuk, A. Mukambaeva, V. Turova, I. Sidorenko, R. Lampe, Influence of the endothelial surface layer on blood flow in microvessels: computer modeling and simulation, CEUR Workshop Proc. 2783 (2020) 153–162.
[20] H.H. Lipowsky, S. Kovalcheck, B.W. Zweifach, The distribution of blood rheological parameters in the microvasculature of cat mesentery, Circ. Res. 43 (5) (1978) 738–749.
[21] H.H. Lipowsky, S. Usami, S. Chien, In vivo measurements of apparent viscosity and microvessel hematocrit in the mesentery of the cat, Microvasc. Res. 19 (3) (1980) 297–319.
[22] A. Lücker, T.W. Secomb, B. Weber, P. Jenny, The relation between capillary transit times and hemoglobin saturation heterogeneity, Part 1: Theoretical models, Front. Physiol 9 (2018) 420.
[23] A. Marki, J.D. Esko, A.R. Pries, K. Ley, J. Leukoc, Role of the endothelial surface layer in neutrophil recruitment, J. Leukoc. Biol2015, 98, 4, 503–515
[24] J.H. Meek, L. Tyszczuk, C.E. Elwell, J.S. Wyatt, Cerebral blood flow increases over the first three days of life in extremely preterm neonates, 1998, Arch. Dis. Child. Fetal Neonatal Ed. 78, F33–F37.
[25] C.E. McLaren, G.M. Brittenham, V. Hasselblad, Statistical and graphical evaluation of erythrocyte volume distributions, Am.J. Physiol 252 (1987). H857–H866
[26] P. Mongan, S. G. Soriano III, T.B. Sloan, A Practical Approach to Neuroanesthesia, Wolters Kluwer, Philadelphia, 2013.
[27] S.K. Piechnik, P.A. Chiarelli, P. Jezzard, Modelling vascular reactivity to investigate the basis of the relationship between cerebral blood volume and flow under CO2 manipulation, Neuroimage 39 (2008) 107–118.
[28] A.R. Pries, T.W. Secomb, T. Gessner, M. Sperandio, J.F. Gross, P. Gaehtgens, Resistance to blood flow in microvessels in vivo, Circ. Res. 75 (1994) 904–915.
[29] A.R. Pries, T.W. Secomb, H. Jacobs, M. Sperandio, K. Osterloh, P. Gaehtgens, Microvascular blood flow resistance: role of endothelial surface layer, Am.J. Physiol 273 (1997) H2272–H2279.
[30] A.R. Pries, T.W. Secomb, P. Gaehtgens, The endothelial surface layer,, Pflug. Arch. – Eur. J. Physiol 440 (2000) 653–666.
[31] A.R. Pries, T.W. Secomb, Microvascular blood viscosity in vivo and the endothelial surface layer, Am. J. Physiol. Heart. Circ. Physiol. 289 (2005). H2657–H2664
[32] A.R. Pries, T.W. Secomb, Blood viscosity in microvessels: experiment and theory, Comptes Rendus Physique. 14 (6) (2013) 470–478.
[33] A. Puchwein-Schwepcke, S. Artmann, L. Rajwich, O. Genzel-Boroviczény, C. Nussbaum, Effect of gestational age and postnatal age on the endothelial glycocalyx in neonates, Sci. Reports 11 (1) (2021) 3133.
[34] B.P. Reines, B.W. Ninham, Structure and function of the endothelial surface layer: unraveling the nanoarchitecture of biological surface, Q. Rev. Biophys. 52 (2019). E13
[35] T.W. Secomb, Blood flow in the microcirculation, Annu. Rev. Fluid Mech. 49 (2017) 443–461.
[36] I. Sidorenko, V. Turova, N. Botkin, L. Eckardt, A. Alves-Pinto, U. Felderhoff-Müser, E. Rieger-Fackeldey, A. Kovtanyuk, R. Lampe, Modeling cerebral blood flow dependence on carbon dioxide and mean arterial blood pressure in the immature brain with accounting for the germinal matrix, Front. Neurol. 9 (2018) 812.
[37] J.R. Skinner, D.W. Milligan, S. Hunter, E.N. Hey, Central venous pressure in the ventilated neonate, Arch. Dis. Child. 67 (4) (1992) 374–377.
[38] M.L. Smith, D.S. Long, E.R. Damiano, K. Ley, Near-wall μ-PIV reveals a hydrodynamically relevant endothelival surface layer in venules in vivo, Biophys. J. 85 (2003) 637–645.
[39] J.M. Squire, M. Chew, G. Nneji, C. Neal, J. Barry, C. Michel, Quasi-periodic substructure in the microvessel endothelial glycocalyx: a possible explanation for molecular filtering? J. Struct. Biol. 136 (2001) 239–255.
[40] V.N. Starovoitov, Behavior of a rigid body in an incompressible viscous fluid near a boundary, in: P. Colli, C. Verdi, A. Visintin (Eds.), Free Boundary Problems. ISNM Int. Series Num. Math., volume 147, 2003, pp. 313–327. Birkhüuser, Basel
[41] M. Tabata, Finite element analysis of axisymmetric flow problems and its application, Circ. Res. 79 (1996) 581–589.
[42] D. Tsvirkun, A. Grichine, A. Duperray, C. Misbah, L. Bureau, Microvasculature on a chip: study of the endothelial surface layer and the flow structure of red blood cells, Sci. Rep. 7 (2017) 45036.
[43] H. Vink, B.R. Duling, Identification of distinct luminal domains for macromolecules, erythrocytes, and leukocytes within mammalian capillaries, Circ. Res. 79 (1996) 581–589.
[44] H. Vink, B.R. Duling, Capillary endothelial surface layer selectively reduces plasma solute distribution volume, Am. J. Physiol. Heart Circ. Physiol. 278 (2000). H285–H289
[45] F.J.M. Walters, Intracranial pressure and cerebral blood flow, Update in Anaesthesia 8 (1998) 18–23.
[46] S. Weinbaum, J.M. Tarbell, E.R. Damiano, The structure and function of the endothelial glycocalyx layer, Annu. Rev. Biomed. Eng. 9 (2007) 121–167.
[47] B.W. Zweifach, H.H. Lipowsky, Quantitative studies of microcirculatory structure and function, III. Microvascular hemodynamics of cat mesentery and rabbit omentum, Circ. Res. 41 (1977) 380–390.